View metadata, citation and similar papers at core.ac.uk

brought to you by CORE

provided by Institutional Research Information System University of Turin

Journal of Solid State Chemistry 194 (2012) 135–142

Contents lists available at SciVerse ScienceDirect

Journal of Solid State Chemistry

journal homepage: www.elsevier.com/locate/jssc

# Location of MTBE and toluene in the channel system of the zeolite mordenite: Adsorption and host–guest interactions

Rossella Arletti [a,*], Annalisa Martucci [b], Alberto Alberti [b], Luisa Pasti [c], Marianna Nassi [c], Roberto Bagatin [d]

[a] Department of Earth Sciences, University of Torino Via Valperga Caluso 35, I-10125, Torino, Italy
[b] Department of Earth Sciences, University of Ferrara, Via G. Saragat 1, I-44100, Ferrara, Italy
[c] Department of Chemistry, University of Ferrara, Via L. Borsari 26, I-44100 Ferrara, Italy
[d] Research Centre for Non-Conventional Energy—Istituto ENI Donegani, Environmental Technologies, Via Fauser 4, I-28100 Novara, Italy

ARTICLE INFO

*Article history:*
Received 30 January 2012
Received in revised form
6 April 2012
Accepted 15 April 2012
Available online 11 May 2012

*Keywords:*
Zeolite mordenite
Structural study
Adsorption
Toluene
MTBE

ABSTRACT

This paper reports a study of the location of Methyl Tertiary Butyl Ether (MTBE) and toluene molecules adsorbed in the pores of the organophylic zeolite mordenite from an aqueous solution. The presence of these organic molecules in the zeolite channels was revealed by structure refinement performed by the Rietveld method. About 3 molecules of MTBE and 3.6 molecules of toluene per unit cell were incorporated into the cavities of mordenite, representing 75% and 80% of the total absorption capacity of this zeolite. In both cases a water molecule was localized inside the side pocket of mordenite. The saturation capacity determined by the adsorption isotherms, obtained by batch experiments, and the weight loss given by thermogravimetric (TG) analyses were in very good agreement with these values. The interatomic distances obtained after the structural refinements suggest MTBE could be connected to the framework through a water molecule, while toluene could be bonded to framework oxygen atoms. The rapid and high adsorption of these hydrocarbons into the organophylic mordenite zeolite makes this cheap and environmental friendly material a suitable candidate for the removal of these pollutants from water.

© 2012 Elsevier Inc. All rights reserved.

## 1. Introduction

Hydrocarbons and halogenated compounds are organic pollutants in industrial waste, especially in waste water deriving from oil refineries, petrochemical plants, and even from common petrol stations. The effective removal of these pollutants from waste water is a problem of great importance and interest and despite significant efforts in environmental restoration over the past 30 years, it remains one of the more difficult and expensive environmental problems. Physical adsorption has proven to be one of the most efficient methods for quickly lowering the concentration of pollutants in waste water [1]. Activated carbons have been the most commonly used adsorbents [2], but they present some disadvantages in that they are relatively expensive, difficult to regenerate, and their performance in removing pollutants is greatly reduced in the presence of natural organic matter, leading to competitive-adsorption effects [3]. Inorganic adsorbents with a high surface area and hydrophobic behavior represent a promising alternative to carbon adsorbents [1,4–8].

Recently, porous materials such as zeolites have been used as sorbents for water treatment, due to their environmentally friendly nature. Zeolites are crystalline aluminosilicates with unique microporosity properties. Their frameworks, built from $SiO_4$ and $AlO_4$ tetrahedral units, present nanometer-sized channels and cages. Their adsorption properties are strongly dependent not only on pore dimensions but also on their chemical properties. The Silica/Alumina ratio is a fundamental parameter that defines zeolite polarity and influences the hydrophobicity or hydrophilicity of each zeolite. While the thermodynamics and kinetics of gas phase adsorption of organic molecules by zeolites has been widely investigated [9], studies of adsorption of organic molecules from aqueous solutions by zeolites are less numerous [5,6,10–15]. Adsorption from aqueous solutions depends not only on the dimension of the pore systems, but also on the competition between the adsorbate and water, strictly linked to the hydrophobicity of the zeolite considered. Databases for correlations between adsorption capacity and pore volume in a given pore size range are limited to very few compounds [11]. Moreover, the knowledge of such parameters may not be sufficient to model and predict adsorption properties. Understanding the science behind adsorption processes helps the operators to design a system that exploits the full capability of adsorbent materials.

* Corresponding author. Fax: +39 011 6705128.
*E-mail address:* rossella.arletti@unito.it (R. Arletti).

0022-4596/$ - see front matter © 2012 Elsevier Inc. All rights reserved.
http://dx.doi.org/10.1016/j.jssc.2012.04.024

The aims of this work are: (i) to investigate the adsorptive properties of mordenite (framework type MOR) for the removal of Methyl Tertiary Butyl Ether (MTBE) and toluene (TOL), two organic pollutants often found in ground and surface water; (ii) to define the structure of the zeolite after the adsorption treatment of the organic molecules and (iii) to comprehend the interaction between the adsorbate and the zeolite framework. A knowledge of the interaction between adsorbent and adsorbate will provide an understanding of the properties of the selected zeolite and be useful for design an adsorbent with high capacity and selectivity. Recent studies [13,15,16] have already highlighted the effectiveness of the zeolite mordenite for the removal of MTBE, but a structural study for the definition of the host–guest interactions is completely lacking. Hung and Lin [16] studied the absorption of MTBE from natural water onto mordenite in comparison with carbonaceous resins. Among the samples tested, one of the resins and mordenite emerged as the most effective adsorbents for MTBE, it being demonstrated that for these two sorbents there was no competition between the organic matter, commonly dispersed in natural water, and the MTBE molecules. Anderson [13] showed that, after equilibration of a 100 $\mu g\,L^{-1}$ MTBE solution with 5 mg of solid phase mordenite powder, the percentage of removal of the pollutant was about 96%. When mordenite is substituted with other zeolites (i.e. ZSM-5 and Y), this percentage falls to 63% and 5% respectively. Unfortunately, the lack of a structural investigation of the MOR powder after adsorption made it impossible to fully explain this high affinity. MTBE molecule dimensions are such that it can fit equally in the channels of both MOR and ZSM-5 (being the longer radius C–C 3.66 Å). The reason for a more efficient removal by MOR must lie in interactions of the molecule with the mordenite framework. Recently, silicalite-1, its polymeric modification and granular activated compound [17] have also been used for MTBE removal. The results, demonstrated high affinity of zeolites for MTBE molecules when compared with other materials. Recently it has been demonstrated that mordenite is an effective mean to remove other pollutant molecules from water, such as 1,2-dichloroethane [14]. In this paper Martucci et al. [14] show that 2.5 DCE molecules can be hosted in the mordenite channel system This relevant incorporation of DCE molecules caused a remarkable increase in the dimension of the 12-ring, when compared to the parent zeolite. As stated above, while some data on MTBE adsorption in mordenite has been published, to the knowledge of the authors no data are available regarding toluene (whose dimensions $4.3 \times 2.4$ Å are such that it can fit in the MOR channels) adsorption by this zeolite. For this reason, in this study the adsorption capacity, the affinity of MOR with MTBE and toluene, and the interaction of the two molecules with the framework are discussed in detail.

## 2. Experimental

### 2.1. Materials

As stated in the introduction, two pollutants were chosen for this study: Methyl Tertiary Butyl Ether (MTBE) and toluene. These two molecules are contaminants found in urban rain water, ground water, and surface water. MTBE is an additive whereas toluene is a component of fuel and they are commonly present in waste water derived from oil refineries and petrochemical plants. MTBE has been found both in drinking and in natural water at different concentrations. Currently, MTBE is listed on EPA's Drinking Water Contaminant Candidate List and drinking water levels have been set at 20 $\mu g\,L^{-1}$ for odor and 40 $\mu g\,L^{-1}$ for taste (EPA, 2002). In groundwater, levels of contamination over 100 $mg\,L^{-1}$ are not uncommon due to spills at automobile gasoline service stations. In particular, Methyl Tertiary Butyl Ether is a primary constituent of reformulated gasoline, accounting for 10–15% of reformulated fuels. Although the health issues associated with exposure to MTBE are still debated, evidence supports its role as a possible human carcinogen [13,18]. MTBE and toluene standard solutions were prepared using purified water from a MilliQ water purification system (Millipore, DA, USA) together with MTBE (HPLC grade, Fisher Scientific, PA, USA) or toluene (HPLC grade, Sigma Adrich, Steinheim, Germany). Sodium chloride (purity 98%) was obtained from Sigma-Aldrich (Steinheim, Germany). The zeolite chosen as sorbent was a commercial as-synthesized hydrophobic mordenite (referred to below as MOR), with $SiO_2/Al_2O_3$ equal to 200 and $Na_2O$ content lower than 0.1 wt%, and purchased from HSZ-690HOA Tosoh Corporation in its protonated forms.

The crystal structure of mordenite was first determined by Meier [19] in 1961. The framework can be described as the assembly of single 6-ring sheets linked by single 4-rings, or, alternatively, from a combination of 5–1 secondary building units (SBUs). A pore system, consisting of 12-membered and 8-membered rings of $TO_4$ tetrahedra, runs parallel to the [001] direction. This channel system is interconnected along [010] through 8-ring side pockets. The topological symmetry of mordenite is orthorhombic *Cmcm* [20], with four symmetrically independent tetrahedral cation sites and ten framework oxygen sites. The real symmetry is reduced to $Cmc2_1$ [21] in the natural phase in order not to constrain one oxygen in an inversion center, and consequently to avoid a straight, unstable T–O–T angle.

### 2.2. Methods

#### 2.2.1. Batch experiments

In order to obtain adsorption equilibrium isotherm data for the powder sorbent, aqueous phase adsorption experiments were performed in 25 mL crimp top reaction glass flasks sealed with PTFE septa (Supelco, PA, USA) using a fixed sorbent/liquid ratio (0.1 g sorbent/25 mL aqueous solution) and initial solutions of varied concentrations of MTBE and toluene, respectively. In all experiments, the flasks were agitated on a fixed speed rotator (200 rpm) at room temperature ($25 \pm 2$ °C) for a minimum of 24 h to achieve adsorption equilibrium. A 24 h equilibration time was chosen on the basis of kinetics testing conducted as part of this work. In addition, previous work on powdered zeolite showed that 24 h is sufficient time for MTBE to reach equilibrium [8]. Control experiments were performed periodically together with the adsorption experiments, using blank solutions of MTBE and toluene and no adsorbent material, to ensure that losses did not occur during the experiments. Following adsorption, solid–liquid separation was achieved by centrifugation for 10 min at 10000 rpm, and MTBE or toluene in the aqueous supernatant samples was quantified using gas chromatography (GC) with solid phase microextraction (SPME) in the headspace mode. When necessary, dilution was made in order to keep the measurements within the linear range of the standard curves.

### 2.3. Gas chromatography

A solid phase microextraction (SPME) system, supplied by Supelco, PA, USA was used to extract the organic contaminant (MTBE or toluene) from the aqueous phase of each sample using carboxen/polydimethylsiloxane (CAR/PDMS) 85 μm film thickness fibers (Supelco, Bellefonte, PA). At the beginning of each analysis, the SPME fiber was conditioned under helium for half an hour in the injector unit at 250 °C and was systematically cleaned at 250 °C for 20–30 min after every extraction. The headspace (HS) mode was used for extraction from a sample volume of 10 ml

of contaminant solutions. The addition of an inorganic salt is common in order to enhance the activity coefficients of volatile components in aqueous solutions, increasing the concentration in the headspace vapor. In the present work, 2 mL of a sodium chloride solution (300 g $L^{-1}$) were added to the sample which was placed in 25 mL glass flasks sealed with Teflon screw caps. After equilibration at 40 ($\pm$0.5) °C, for 10 min, the SPME was inserted and the samples were maintained under controlled agitation with a magnetic stirrer (300 rpm) for 10 min. Finally, the fiber was inserted into the GC injector for analysis. The desorption time was 1 min. A GC HRGC 5160 MEGA SERIES Instrument (Carlo Erba, Mi, I) equipped with a split/splitless injector, a flame ionization detector (FID) and a fused-silica SE30 capillary column (60 m × 0.25 mm I.D:, 0.25 μm film thickness; J&W Scientific, USA) was employed in this work. Helium (99.999%) was used as a carrier gas at a constant head pressure of 50 kPa. The detector and injector temperatures were held constant at 250 °C. Hydrogen and air were used to maintain the detector flame at a pressure of 40 and 80 KPa, respectively. The GC oven program was as follows: 35 °C for 1 min, ramped to 50 °C at 7.5 °C $min^{-1}$, held for 2 min, ramped to 90 °C at 20 °C $min^{-1}$, held for 2 min, and finally ramped to 200 °C at 40 °C $min^{-1}$ and held for 10 min. The MTBE (or toluene) on the SPME fiber was thermally desorbed in the GC inlet using the splitless mode at 250 °C for 5 min. The linearity of the method for quantitative analysis was tested by the evaluation of the calibration curves: standard solutions of MTBE and toluene in MilliQ water were analyzed at varying concentration levels in the range 0.01–10 ppm as single contaminants. Each concentration was analyzed twice. The linearity range was evaluated, as well as the method detection limit (LOD) and computed from the calibration line. Good linearity was observed with a correlation coefficient of 0.9952 and 0.9984 for MTBE and toluene respectively. Exhausted MTBE and toluene mordenite samples were prepared by repeating batch adsorption steps on the same zeolite sample, until the concentration of the solution in contact with the zeolites did not change. The concentration of the organics in the aqueous solution was analyzed by HS–SPME–GC and this operation was repeated until the concentration of MTBE or toluene in the solution did not decrease after contact with the zeolite. These exhausted samples will be indicated below as MTBE–MOR and TOL–MOR.

### 2.4. X-ray powder diffraction analyses

X-Ray powder diffraction patterns (XRPD) were collected at room temperature on untreated mordenite, MTBE–MOR, and TOL–MOR. The experiments were carried out on a Bruker D8 Advance diffractometer, with Bragg–Brentano $\theta$–$\theta$ geometry, equipped with a Sol–X detector using Cu$K_{\alpha1,\alpha2}$ radiation. The spectra were collected in the $2\theta$ range 3–115° with a 0.02° step and counting times of 12 s/step. Rietveld profile fitting was performed on all the spectra using the GSAS package [22], with the EXPGUI [23] interface. The powder patterns of the untreated and two exhausted mordenites are reported in Fig. 1. Structural details of untreated mordenite can be found in Martucci et al. [24] or asked to those authors since the mordenite sample studied here was the same as used in [24]. The coordinates used in [24] were taken as starting coordinates for the exhausted MTBE–MOR sample refinement, while those from Alberti et al. [21] were used for the TOL–MOR sample, for the reason reported in Section 3. The background curve was fitted by a Chebyshew polynomial with an average of 20 coefficients. The pseudo-Voigt profile function proposed by Thomson et al. [25] and peak intensity cut-off were applied. The $2\theta$–zero shift, the scale factor and unit-cell parameters were allowed to vary for all the histograms. The refined structural parameters for each data histogram were the following: fractional coordinates and isotropic displacement factors for all atoms and occupancy factors for the extraframework atoms. Occupancy factors and isotropic displacement factors were varied in alternate cycles. The isotropic displacement parameters were constrained in the following way: the same value for all tetrahedral cations, a second value for all framework O atoms, and a third value for all the extra-framework sites. Soft restraints were applied to the T–O distances [Si–O = 1.60(2) − 1.63(2)] and the weight was gradually decreased after the initial stages of refinement, down to 10. The crystallographic data and refinement details are reported in Table 1. Tables 2 and 3 report the final atomic positions, thermal parameters, and occupancies of MTBE–MOR and TOL–MOR, respectively. The interatomic distances and angles are listed in Tables 4 and 5.

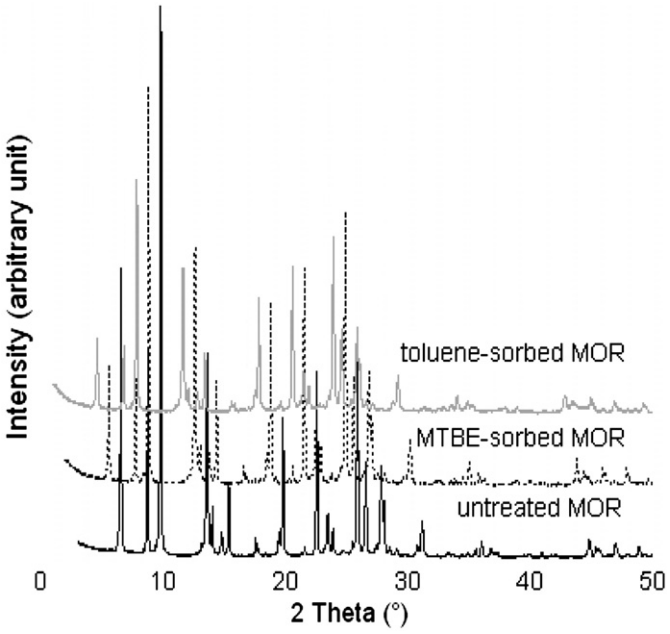


**Fig. 1.** XRPD patterns of untreated, MTBE-sorbed and toluene-sorbed mordenite (the stacked plots have been shifted for easy comparison).

**Table 1**
Lattice parameters and Rietveld refinement details before (MOR, data from Martucci et al. [24]), and after MTBE (MTBE–MOR) and toluene (TOL–MOR) adsorption.

| | **MOR** [24] | **MTBE–MOR** | **TOL–MOR** |
|---|---|---|---|
| **Space group** | *Cmcm* | *Cmcm* | $Cmc2_1$ |
| ***a*** **(Å)** | 18.069(1) | 18.0572(6) | 18.0709(9) |
| ***b*** **(Å)** | 20.219(1) | 20.2323(6) | 20.2372(8) |
| ***c*** **(Å)** | 7.456(3) | 7.4572(2) | 7.4577(3) |
| ***V*** **(Å$^3$)** | 2723.9(2) | 2724.3(1) | 2727.3(2) |
| $R_{wp}$ | – | 14.05 | 12.03 |
| $R_p$ | – | 11.05 | 9.08 |
| $R_F^2$ | – | 9.2 | 10.04 |
| ***N*° reflections** | – | 2204 | 2295 |
| ***N*° obs** | – | 5674 | 5680 |
| ***N*° variables** | – | 87 | 114 |

### 2.5. Thermal analyses

Thermogravimetric (TG) and differential thermal analysis (DTA) measurements of both as-synthesized and exhausted samples were performed in air up to 900 °C using an STA 409

**Table 2**
MTBE–MOR atomic coordinates, occupancies (*F*) and displacement parameters (Uiso $Å^2 \times 100$).

| | *x/a* | *y/b* | *z/c* | *F* | Uiso |
|---|---|---|---|---|---|
| **Si1** | 0.3054(3) | 0.0730(2) | 0.0416(7) | 1.0 | 0.0274(9) |
| **Si2** | 0.3049(3) | 0.3113(2) | 0.0423(6) | 1.0 | 0.0274(9) |
| **Si3** | 0.0860(4) | 0.3812(4) | 0.25 | 1.0 | 0.0274(9) |
| **Si4** | 0.0828(5) | 0.2223(4) | 0.25 | 1.0 | 0.0274(9) |
| **O1** | 0.1204(5) | 0.4084(5) | 0.4343(10) | 1.0 | 0.032(2) |
| **O2** | 0.1226(5) | 0.1891(6) | 0.4199(12) | 1.0 | 0.032(2) |
| **O3** | 0.2349(4) | 0.1187(4) | 0.9949(14) | 1.0 | 0.032(2) |
| **O4** | 0.0887(8) | 0.3017(4) | 0.25 | 1.0 | 0.032(2) |
| **O5** | 0.1704(8) | 0.1876(11) | 0.75 | 1.0 | 0.032(2) |
| **O6** | 0.1702(9) | 0.4194(9) | 0.75 | 1.0 | 0.032(2) |
| **O7** | 0.2254(7) | 0.50 | 0.50 | 1.0 | 0.032(2) |
| **O8** | 0.25 | 0.25 | 0.5 | 1.0 | 0.032(2) |
| **O9** | 0.00 | 0.4026(11) | 0.25 | 1.0 | 0.032(2) |
| **O10** | 0.00 | 0.1930(11) | 0.25 | 1.0 | 0.032(2) |
| **C1** | 0.50 | 0.393(4) | 0.25 | 0.74(2) | 0.38(3) |
| **C2** | 0.50 | 0.469(4) | 0.25 | 0.74(2) | 0.38(3) |
| **C3** | 0.422(2) | 0.5019(34) | 0.25 | 0.74(2) | 0.38(3) |
| **C4** | 0.00 | 0.063(5) | 0.042(3) | 0.39(2) | 0.38(3) |
| **O11** | 0.00 | −0.001(4) | 0.080(1) | 0.39(2) | 0.38(3) |
| **W1** | 0.481(7) | 0.2368(25) | 0.25 | 0.33(1) | 0.38(3) |

**Table 3**
TOL–MOR atomic coordinates, occupancies (*F*) and displacement parameters (Uiso $Å^2 \times 100$).

| | *x/a* | *y/b* | *z/c* | *F* | Uiso |
|---|---|---|---|---|---|
| **Si1** | 0.3076(10) | 0.0740(15) | 0.04326 | 1 | 0.0078(8) |
| **Si1a** | 0.6991(10) | 0.9267(15) | 0.9539(16) | 1 | 0.0078(8) |
| **Si2** | 0.3060(13) | 0.3114(13) | 0.043(4) | 1 | 0.0078(8) |
| **Si2a** | 0.6950(13) | 0.6889(13) | 0.964(4) | 1 | 0.0078(8) |
| **Si3** | 0.0850(6) | 0.3811(5) | 0.233(3) | 1 | 0.0078(8) |
| **Si4** | 0.0849(5) | 0.2232(5) | 0.244(4) | 1 | 0.0078(8) |
| **O1** | 0.1226(15) | 0.4033(20) | 0.420(4) | 1 | 0.0068(1) |
| **O1a** | 0.8777(16) | 0.5877(19) | 0.558(5) | 1 | 0.0068(1) |
| **O2** | 0.1260(14) | 0.1861(16) | 0.408(4) | 1 | 0.0068(1) |
| **O2a** | 0.8840(14) | 0.8039(19) | 0.554(4) | 1 | 0.0068(1) |
| **O3** | 0.2345(17) | 0.1181(15) | 0.006(5) | 1 | 0.0068(1) |
| **O3a** | 0.7707(17) | 0.8851(14) | 0.020(5) | 1 | 0.0068(1) |
| **O4** | 0.0895(7) | 0.3028(5) | 0.260(5) | 1 | 0.0068(1) |
| **O5** | 0.1675(8) | 0.1917(11) | 0.754(4) | 1 | 0.0068(1) |
| **O6** | 0.1621(9) | 0.4189(8) | 0.7522(17) | 1 | 0.0068(1) |
| **O7** | 0.2251(8) | 0.4986(16) | 0.498(6) | 1 | 0.0068(1) |
| **O8** | 0.2487(23) | 0.2524(18) | 0.518(6) | 1 | 0.0068(1) |
| **O9** | 0 | 0.4115(11) | 0.240(9) | 1 | 0.0068(1) |
| **O10** | 0 | 0.1945(13) | 0.245(10) | 1 | 0.0068(1) |
| **W1** | 0.5 | 0.231(1) | 0.250(11) | 0.90(2) | 0.129(2) |
| **C1** | 0.5413(2) | 0.427(1) | 0.096(5) | 0.89(1) | 0.062(9) |
| **C2** | 0.5414(2) | 0.545(1) | 0.140(4) | 0.89(1) | 0.062(9) |
| **C3** | 0.5867(7) | 0.484(1) | 0.165(5) | 0.89(1) | 0.062(9) |

PC LUXX®—Netzch at 10 °C $min^{-1}$ heating rate. The TG plots are reported in Fig. 2.

## 3. Results and discussion

### 3.1. Batch experiments

The adsorption data of MTBE and toluene in water on mordenite vs. time is reported in Fig. 3. It can be seen that in both cases equilibrium was reached within few minutes. The equilibration time employed in the batch experiments is, however, longer, since it was found that differences in adsorption arise from short time contact [26]. The pollutant (MTBE or TOL) concentrations in contact with the sorbent at the equilibrium are indicated as $c_e$. Fig. 4 shows the MTBE and TOL sorption isotherms at room temperature (25 °C) for mordenite. In Fig. 4a and b, $q$, the adsorbed concentration i.e. the mass of adsorbed pollutant per gram of sorbent ($mg\,g^{-1}$) vs. $_e$ the equilibrium concentrations ($mg\,L^{-1}$) are reported. The adsorbed concentration $q$ is obtained as

$$q = \frac{(c_o - c_e)V}{w} \quad (1)$$

where $V$ is the volume of pollutant aqueous solution (L) and $w$ the weight (g) of adsorbent material.

The initial concentrations ($c_0$) placed in contact with the sorbent included the $\mu g\,L^{-1}$ range up to the $0.1\,g\,L^{-1}$ range. The latter concentrations are seldom found in natural water, however, in adsorption studies a wider concentration range can be useful to better define the adsorption isotherm [27]. The data in the low concentration range showed that the isotherm is linear (see Fig. 4b). Only when the concentration increases is a limiting sorption capacity observed, as reported in Fig. 4a. At high concentrations the sorbent become saturated, due to the limited space in the sorbent material available to host MTBE molecules. These results were interpreted by Giaya et al. [28] as consistent with the hypothesis of partition of the organic molecules between the water phase and the sorbent, with adsorption favoured by the environment created by the hydrophobic pore surfaces.

A similar trend was also observed for the adsorption of toluene on mordenite (see Fig. 4a and b). The data were fitted using a Langmuir equation

$$q = \frac{q_S K_L c_e}{1 + K_L c_e} \quad (2)$$

where $q_S$ is the saturation capacity, ($mg\,L^{-1}$) and $K_L$ the equilibrium association constant ($L\,mg^{-1}$), and a Freundlich

**Table 4**
T–O framework distances (Å) and selected interatomic distances for MTBE–MOR.

| | | Distance | | Angle | Degrees |
|---|---|---|---|---|---|
| **Si1** | **O1** | 1.604(4) | | **O1–Si1–O3** | 114.7(7) |
| | **O3** | 1.611(4) | | **O1–Si1–O6** | 103.3(6) |
| | **O6** | 1.622(4) | | **O1–Si1–O7** | 114.0(7) |
| | **O7** | 1.610(4) | | **O3–Si1–O6** | 111.5(9) |
| | | | | **O3–Si1–O7** | 102.2(5) |
| **Si2** | **O2** | 1.595(4) | | **O6–Si1–O7** | 111.4(8) |
| | **O3** | 1.612(4) | | | |
| | **O5** | 1.612(3) | | **O2–Si2–O3** | 105.8(6) |
| | **O8** | 1.619(3) | | **O2–Si2–O5** | 108.9(6) |
| | | | | **O2–Si2–O8** | 112.8(6) |
| **Si3** | **O1** | 1.606(3) | | **O3–Si2–O5** | 106.1(9) |
| | **O1** | 1.606(3) | | **O3–Si2–O8** | 111.4(5) |
| | **O4** | 1.609(4) | | **O5–Si2–O8** | 111.6(8) |
| | **O9** | 1.612(4) | | | |
| | | | | **O1–Si3–O1** | 117.6(10) |
| **Si4** | **O2** | 1.604(3) | | **O1–Si3–O4** | 109.4(5) |
| | **O2** | 1.604(3) | | **O1–Si3–O9** | 106.3(4) |
| | **O4** | 1.609(4) | | **O1–Si3–O4** | 109.4(5) |
| | **O10** | 1.609(4) | | **O1–Si3–O9** | 106.3(4) |
| | | | | **O4–Si3–O9** | 107.4(12) |
| **C1** | **C2** | 1.552(4) | | | |
| | | | | **O2–Si4–O2** | 104.3(10) |
| **C2** | **C3** | 1.552(4) | × 2 | **O2–Si4–O4** | 112.9(7) |
| | **O11** | 1.410(5) | | **O2–Si4–O10** | 105.2(4) |
| | | | | **O2–Si4–O4** | 112.9(7) |
| **C3** | **C2** | 1.552(4) | | **O2–Si4–O10** | 105.2(4) |
| | **O11** | 2.499(4) | | **O4–Si4–O10** | 115.3(12) |
| **O11** | **C4** | 1.552(4) | | | |
| | **C2** | 1.410(5) | | | |
| **C4** | **O11** | 1.552(4) | | | |
| **W1** | **C1** | 3.17(2) | | | |
| | **O5** | 3.13(4) | | | |

**Table 5**
T–O framework distances (Å) and selected interatomic distances for TOL–MOR.

| | | Distance | Angle | Degrees |
|---|---|---|---|---|
| **Si1** | **O1** | 1.626(10) | **O1–Si1–O3** | 112.3(23) |
| | **O3** | 1.620(10) | **O1–Si1–O6** | 104.5(17) |
| | **O6** | 1.658(10) | **O1–Si1–O7** | 115.0(20) |
| | **O7** | 1.618(10) | **O5–Si1–O6** | 112.6(17) |
| | | | **O5–Si1–O7** | 99.6(21) |
| **Si1a** | **O1a** | 1.615(10) | **O9–Si1–O7** | 113.2(22) |
| | **O3a** | 1.620(10) | | |
| | **O6** | 1.653(10) | **O1a–Si1a–O3a** | 116.5(26) |
| | **O7** | 1.618(10) | **O1a–Si1a–O6** | 94.1(18) |
| | | | **O1a–Si1a–O7** | 108.7(20) |
| **Si2** | **O2** | 1.589(10) | **O3a–Si1a–O6** | 123.4(19) |
| | **O3a** | 1.631(10) | **O3a–Si1a–O7** | 101.1(20) |
| | **O5** | 1.645(10) | **O6–Si1a–O7** | 113.1(22) |
| | **O8** | 1.638(10) | | |
| | | | **O2–Si2–O3a** | 102.0(21) |
| **Si2a** | **O2a** | 1.583(10) | **O2–Si2–O4** | 112.5(19) |
| | **O3** | 1.629(10) | **O2–Si2–O9** | 114.9(28) |
| | **O5** | 1.649(10) | **O3a–Si2–O4** | 104.4(20) |
| | **O8** | 1.615(10) | **O3a–Si2–O9** | 118.2(23) |
| | | | **O5–Si2–O9** | 104.6(21) |
| **Si3** | **O1** | 1.617(10) | | |
| | **O1a** | 1.600(10) | **O2a–Si2a–O3** | 113.3(22) |
| | **O4** | 1.599(9) | **O2a–Si2a–O5** | 97.4(16) |
| | **O9** | 1.656(8) | **O2a–Si2a–O8** | 113.3(28) |
| | | | **O3–Si2a–O5** | 110.1(21) |
| **Si4** | **O2** | 1.617(10) | **O3–Si2a–O8** | 108.8(25) |
| | **O2a** | 1.618(10) | **O5–Si2a–O8** | 113.6(23) |
| | **O4** | 1.618(9) | | |
| | **O10** | 1.640(9) | **O1–Si3–O1a** | 114.8(12) |
| | | | **O1–Si3–O4** | 98.4(19) |
| **C1** | **C1** | 1.493(8) | **O1–Si3–O9** | 105.0(22) |
| | **C3** | 1.504(7) | **O1a–Si3–O4** | 118.2(18) |
| | **O2** | 3.100(8) | **O1a–Si3–O9** | 105.7(21) |
| | | | **O4–Si3–O9** | 114.3(13) |
| **C2** | **C2** | 1.497(8) | | |
| | **C3** | 1.492(7) | **O2–Si4–O2a** | 110.1(12) |
| | **O10** | 3.210(8) | **O2–Si4–O4** | 112.5(21) |
| | | | **O2–Si4–O10** | 105.0(23) |
| **C3** | **C1** | 1.504(7) | **O2a–Si4–O4** | 112.7(24) |
| | **C2** | 1.492(8) | **O2a–Si4–O10** | 102.2(26) |
| | **O3a** | 3.441(7) | **O4–Si4–O10** | 113.6(13) |

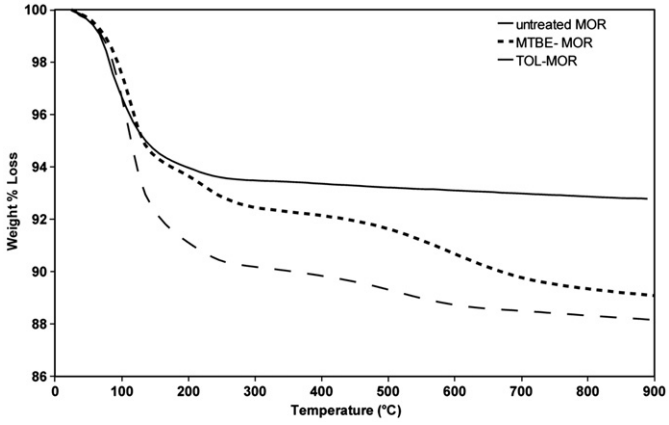


**Fig. 2.** Thermogravimetric analyses of untreated, MTBE-sorbed and toluene-sorbed mordenite.

model

$$q = K_F c_e^{1/n} \quad (3)$$

where $K_F$ is a constant indicative of the adsorption capacity of the adsorbent and $n$ is an empirical constant.

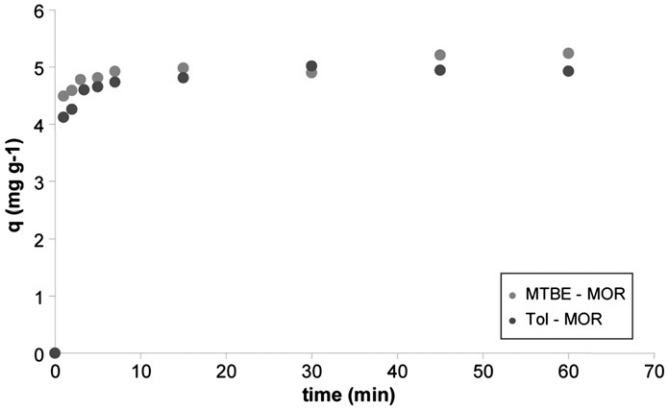


**Fig. 3.** Adsorption kinetics of MTBE and toluene on mordenite.

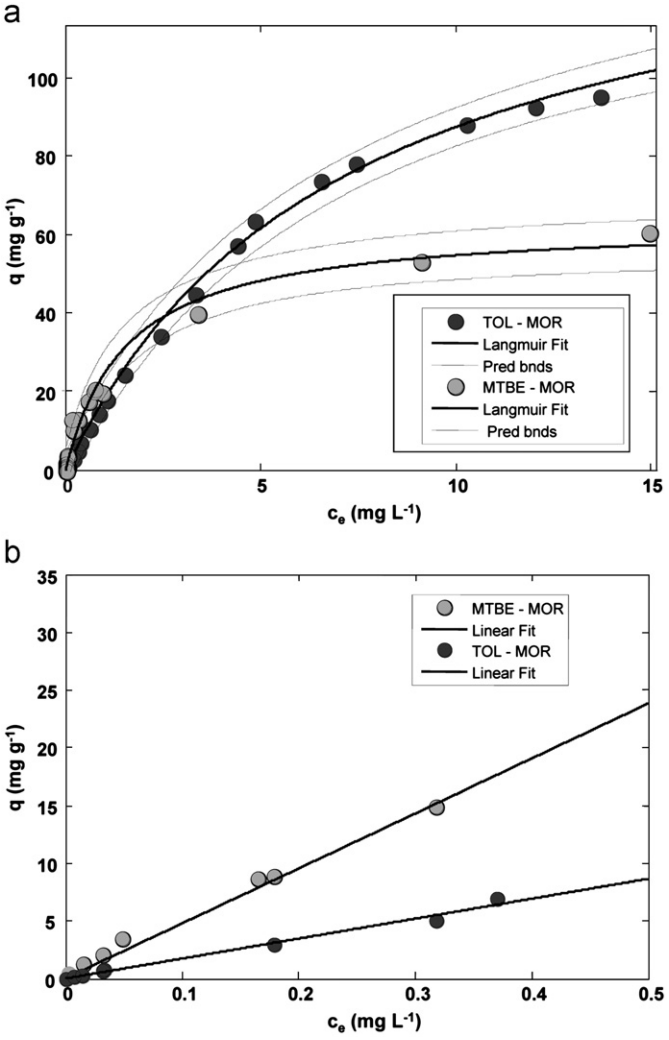


**Fig. 4.** Adsorption isotherm of MTBE and toluene on mordenite; circle symbols: measured equilibrium concentrations; (a) solid line: fitted Langmuir equation; dashed lines: 95% confidence prediction bounds. (b) Solid line: linear fit equation.

In the low concentration range a linear fitting

$$q = Kc_e \quad (4)$$

where $K$ is a constant and is employed. At the low concentration Eq. (2) converges with Eq. (4) with $K$ equal to $K_L q_s$.

The determination coefficients for the two models (i.e. Eqs. (3) and (4)) are not very different from each other (see Table 6); however, the

**Table 6**
Fitted parameters of the isotherm models (see Eqs. (2–4)).

| Zeolite–Organic | Adsorption model | $K_L$ (L mg$^{-1}$) | $q_S$ (mg g$^{-1}$) | $R^2$ |
|---|---|---|---|---|
| MOR–MTBE | Langmuir | 0.293 (0.262, 0.324) | 70.8 (57.0, 84.6) | 0.9826 |
| MOR–Tol | Langmuir | 0.138 (0.117, 0.160) | 150.5 (139.1, 161.9) | 0.9964 |
| | | $K_F$ (mg g$^{-1}$)(L g$^{-1}$)$^n$ | $n$ | $R^2$ |
| MOR–MTBE | Freundlich | 19.4 (18.1, 20.6) | 0.574 (0.552, 0.595) | 0.9935 |
| MOR–Tol | Freundlich | 21.0 (17.8, 24.2) | 0.615 (0.544, 0.686) | 0.9763 |
| | | $K$ | | $R^2$ |
| MOR–MTBE | Linear | 47.6 (44.5, 49.7) | | 0.9832 |
| MOR–Tol | Linear | 17.3 (16.0, 18.6) | | 0.9881 |

latter equation was employed since it has often been used for fitting volatile organic compounds adsorption on zeolites [29]. The fitted saturation capacity of MOR (see Table 6) is higher for toluene than for MTBE. By contrast, in the low concentration range the slope of linear fitting is higher for MTBE than for toluene, indicating a stronger interaction of MTBE with the adsorbent. For the adsorption of MTBE on zeolites it has been proposed that at low MTBE concentrations the dominant factors for favorable sorption are high Silica/Alumina ratio and high framework density (i.e. rather small pores) to disrupt the structure of water and to increase the affinities, while at high MTBE concentrations hydrophobicity and a large pore volume are important to obtain high capacities. Moreover, it has already been observed that the structure of a zeolite and not only the pore dimensions can play an important role in adsorption [24]. Mordenite has an essentially two-dimensional intersecting pore system, constituted by two channel types as previously described in the Section 2.1., the smaller channel could limit MTBE diffusion. Therefore, conclusions about adsorption should be considered in the light of the structures of this material.

### 3.2. Thermogravimetric and structural analysis

#### 3.2.1. MTBE

The thermogravimetric curves (TG) of untreated material and MTBE–MOR are reported in Fig. 2. The TG curve of the untreated material shows a total weight loss of about 7%. The loss shown in the TG curve is due to water molecules weakly bonded to the surface (loss below 100 °C) and water molecules or silanols present inside the channel (loss at higher temperatures). According to the TG analyses, the amount of $H_2O$ bonded to the surface of the grains corresponds to about 3% in weight, while the structural $H_2O$ or OH accounting for the remaining weight loss represent about 4%. TG analysis of MTBE–MOR clearly indicates adsorption, with the TG curve showing a total weight loss at 900 °C of about 11–12% compared to 7% for the untreated powder. At low temperature the TG curve of the treated and untreated samples shows a similar behavior (with a loss around 3% at 100 °C). The residual loss (8–9% in weight) which occurs in MTBE–MOR at higher temperatures (above 200 °C), is probably related to the presence of molecules adsorbed in the mordenite channels.

In X-Ray powder diffraction pattern, no remarkable differences are evidenced in the peak positions between treated and untreated samples (Fig. 1). No violation of the C-centering systematic was observed and the pattern of MTBE–MOR matched satisfactorily with the space group *Cmcm*, which is usually accepted for mordenite. A comparison of the unit cell parameters reported by Martucci et al. [24] with those derived in the present work (Table 1), revealed small differences in the *a* and *b* parameters. The powder diffraction patterns reported in Fig. 1 clearly highlighted that the peak intensities of MOR and MTBE–MOR are markedly different, especially in low angle range. It is well know that in zeolites the intensities of their low-angle diffraction peaks are extremely sensitive to the arrangement and occupancy of extra-framework species. The decrease in the relative intensity of the first peak could be an indication that MTBE molecules entered the zeolite channels and the adsorption process by the MTBE solution induced changes in the MOR structure. The framework model of Martucci et al. [24] was used in the initial stage of Rietveld refinement, which converged readily. At this point, the Difference Fourier map of the electronic density, enabled the location of the MTBE molecule inside the 12-ring channel. In addition, a partially occupied water site was detected. The Rietveld refinement of this model, carried out according to the procedure reported in Section 2., converged, indicating partial occupancies by both MTBE and water molecules. As a whole, 3 MTBE molecules and 2.5 water molecules per unit cell were found.

The structure of the MTBE–MOR is reported in Figs. 5 and 6; the organic molecules are in the 12-membered ring channel, with their symmetry plane on the mirror plane orthogonal to the *a*-axis, whereas the water molecule is located inside the side pocket. Two partially occupied MTBE molecules are symmetrically related by the mirror plane at $z/c=0.25$ leading to two

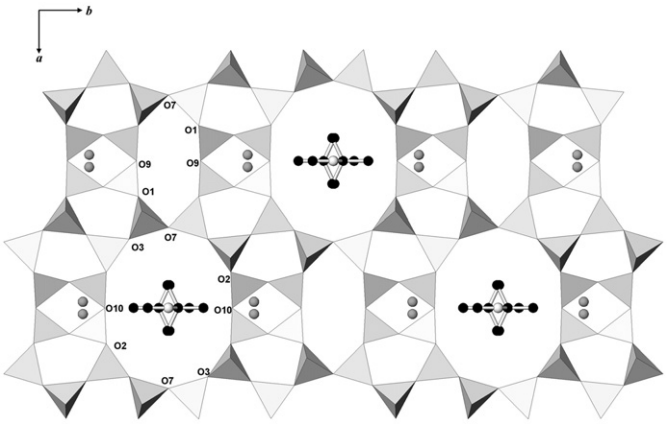


**Fig. 5.** Projection of the MTBE sorbed mordenite along the [001] direction.

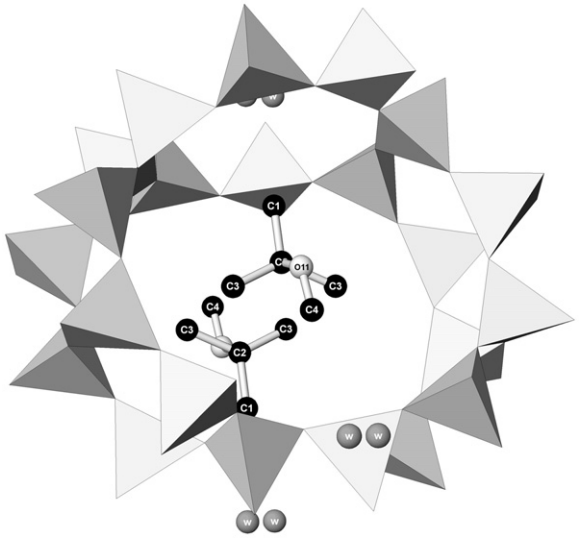


**Fig. 6.** Details of the location of MTBE molecules in the 12-ring channel viewed along [111].

different molecule orientations, with a face of the molecule's tetrahedron (C3–C1–C3 in Tables 2 and 4 and in Figs. 5 and 6) lying on the mirror plane. However, from this refinement the carbon atom C2 which should occupy the center of the tetrahedron of MTBE (Table 2 and Figs. 5 and 6) was found on the mirror plane at $z/c=0.25$, i.e. on the tetrahedron face C3–C1–C3. Therefore a new Rietveld refinement was carried out in the space group $Cmc2_1$, a subgroup of *Cmcm*. Such a symmetry loses the mirror plane orthogonal to *c*, and was invoked by some authors, for the framework of MOR itself [21,30]. It is notable that, owing to the position of the MTBE molecule, *Cmcm* cannot be the real symmetry but only a pseudosymmetric symmetry, with $Cmc2_1$ as the real symmetry. However, after the refinement in this symmetry, the C2 carbon atom was again located at about the center of the C3–C1–C3 face, and the MTBE molecules showed very similar orientation and occupancy, thus justifying the refinement in the topological symmetry *Cmcm*. At this point a Rietveld refinement in the *Cmcm* space group was performed, with the MTBE guest molecule treated as a rigid body. Its conformation was taken from Slovokhotov et al. [31]. These rigid body constrains were progressively reduced and, as a result, the C2 carbon once again shifted up to the position found in the previous refinements. This anomalous result was interpreted as a consequence of the disorder in double configuration of MTBE molecules and the short distance between the position of the two possible C2 carbon atoms, very close to the mirror plane and, consequently, to each other. The high temperature displacement found for the atoms of the MTBE molecule (see Table 2) supports this interpretation.

**Table 7**
Free diameter (Å) of the 12-ring and 8-ring channels and free area (Å$^2$) before (MOR, data from Martucci et al. [24]), and after MTBE (MTBE–MOR) and toluene (TOL–MOR) adsorption.([a] sensu Baerlocher et al. [32]). Labels refer to Fig. 5.

| | | Untreated MOR | MTBE–MOR | TOL–MOR |
|---|---|---|---|---|
| **12-ring** | **O10–O10** | 5.74 | 5.95 | 6.01 |
| | **O3–O3** | 6.91 | 7.05 | 6.92 |
| | **O2–O2** | 6.14 | 6.2 | 6.25 |
| | **O7–O7** | 7.15 | 7.22 | 7.24 |
| | **Free Area** | 33.14 | 34.31 | 36.63 |
| **8-ring** | **O7–O7** | 5.41 | 5.44 | 5.43 |
| | **O9–O9** | 3.01 | 2.72 | 2.47 |
| | **O1–O1** | 3.20 | 3.10 | 3.18 |

The distances of the water molecule from a framework oxygen (W1–O5=3.13 Å) and a carbon atom (W–C1=3.17 Å) (see Table 4) suggest that MTBE molecule could be connected to the framework through water. It is worth noting that the amount of extraframework content (MTBE molecules plus water about 9.7 wt%) found by the structure refinement is in close agreement with the data of TG analyses (8–9 wt%) and adsorption isotherms.

The data reported in Table 7 show the changes in the mordenite channels after MTBE adsorption. The 12-ring channel hosting the organic molecule widens, in particular along the O10–O10 direction (Table 4), an effect justified by the molecule orientation (see Fig. 5). As a consequence of the 12-ring widening, a narrowing and a distortion of the 8-ring channel to accommodate the structural deformations is observed. The small variations noted in the unit cell volume are the consequence of the combined effect of the widening/contraction of the two channels. It is worth noting that the 3 MTBE molecules found by the structure refinement correspond to 75% the adsorption capacity of the mordenite 12-ring channels.

### 3.2.2. Toluene

The TG curve of TOL–MOR reported in Fig. 2, shows that the total weight loss (about 12%) is slightly greater than that for MTBE–MOR. However, the plot show that the two phases behave in a very different way, with the TOL–MOR loss being faster in the early stage of heating compared with the other sample. At about 200 °C the MTBE–MOR loss is about 6%, while TOL–MOR lost more than 9% in weight, which is more than 3/4 of the total loss. The remaining 3% was lost very slowly in the subsequent 600 °C, with the reaction almost completed at 800 °C.

As noted above for the MTBE–MOR sample, the powder diffraction pattern of TOL–MOR reported in Fig. 1 shows variation in the intensities ratio of the peaks at low $2\theta$ angle, probably in relation to the presence of the molecules in the cavities. Even if no new peaks appear in the pattern, the Rietveld refinement suggested a lowering of symmetry. In fact, the $R_F^2$ factor was significantly lower when the structure was refined in the $Cmc2_1$ space group, instead of the *Cmcm* used in the previous refinements. Consequently, the starting coordinates for TOL–MOR refinement were taken from the work of Alberti et al. [21]. The cell parameters obtained after the refinement are reported in Table 1, and it is evident that only slight variations occurred,

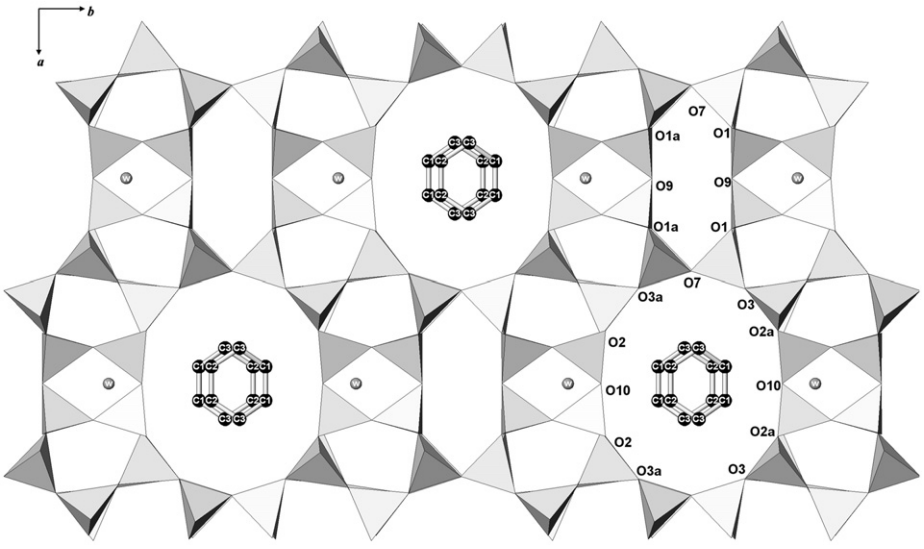


**Fig. 7.** Projection of the toluene sorbed mordenite along the [001] direction.

accounting for a small but significant volume expansion. The Fourier differences maps allow localization of the hexagonal ring of toluene molecule in the 12-ring channel (see Fig. 7). The center of the hexagonal ring of the organic molecule lies on the screw axis running along *c*, so that two different toluene molecules are shifted along the *z*-axis of *c*/2 (at a distance of 3.7 Å) as a consequence of the presence of the screw axis parallel to [001]. It was not possible to unambiguously localize the methyl group, probably because of disorder in its position. It is notable that the toluene molecule is not perpendicular to *c*-axis, as evidenced by the *z*/*c* values of the carbon atoms of the toluene molecule. This tilting explains the loss of the mirror plane orthogonal to [001] and, consequently, the lowering of symmetry from the space group *Cmcm* to the space group $Cmc2_1$, induced by the adsorption of the organic molecules onto the zeolitic pores.

The occupancy factors of the carbon sites (about 0.9 in Table 3) of the hexagonal ring (C1, C2, C3) indicate adsorption of 3.6 toluene molecules per unit cell. This implies that slightly less than two toluene molecules are hosted inside each 12-member channel. Considering the toluene molecule orientation and the *c* parameter of mordenite (about 7.4 Å), no more than two molecules can be hosted in each channel. Consequently, the absorption of toluene in the mordenite zeolite is very near its maximum capacity (3.6 molecules of 4 maximum permitted).

In addition to the organic molecules, a crystallographic site, partially occupied by water molecules (accounting for 3.6 molecules) was located inside the side pocket, very near the water molecule found in MTBE–MOR. Overall, the electron density of the extraframework species corresponds to a total weight of about 12%. This value is in very close agreement with that found from the TG analysis and adsorption isotherm.

The interatomic distances found in the refined structure make it possible to postulate a stronger interaction between toluene and the mordenite framework compared with the MTBE molecule. Even if it was not possible to localize the methyl group, due to its probable statistically disordered position, it can be presumed that its carbon atom should have a distance lower than 3.00 from an oxygen atom of the framework. In fact, the distances of C1 and C2 from the framework oxygen atoms O2 and O10 are 3.10 and 3.21 Å, respectively (see Table 5), and if a methyl group is bonded to one of these carbon atoms the result is an interaction of the molecule with the framework. Considering the geometry of the toluene molecule it is reasonable assume that the methyl group is bonded to C1 and oriented towards framework oxygen O2. Similarly to MTBE adsorption, the presence of the toluene molecules induces a widening of the 12-ring channel with a consequent deformation and narrowing of the 8-ring (see Table 7).

## 4. Conclusions

X-Ray powder diffraction experiments allowed the localization of host molecules and showed a loading of 75% and 80% of the mordenite total capacity for MTBE and toluene respectively. In both the experiments the organic molecules were found to in the 12-membered ring. The short distance between the carbons of the toluene 6-ring and framework oxygen atoms indicated a possible interaction between the molecule and the guest zeolite, whereas a weaker interaction was observed between MTBE molecules and the mordenite framework.

## References

[1] W.T. Tzsai, K.J. Hsien, H.C. Hsu, J. Hazard. Mater. 166 (2009) 635–641.
[2] A. Reife, H.S. Freeman, in: A. Reife, H.S. Freeman (Eds.), Environmental Chemistry of Dyes and Pigments, 1996, pp. 3–31.
[3] T.C. Shih, M. Wangpaichitr, M. Suffet, Water Res. 37 (2003) 375–385.
[4] S.W. Blocky, Environ. Prog. 12 (1993) 223–230.
[5] M. Khalid, G. Joly, A. Renaud, P. Magnoux, Ind. Eng. Chem. Res. 43 (2004) 5275–5280.
[6] H.T. Shu, D. Li, A.A. Scala, Y.H. Ma, Sep. Purif. Technol. 11 (1997) 27–36.
[7] S.J. Allen, in: G. McRay (Ed.), Use of adsorbent for the removal of Pollutants form wastewater, CRC Press, Boca Raton, FL, 1996, pp. 59–97.
[8] W.K. Gupta, I Alli, Encyclopedia of Surface and colloid Science, in: A.T. Hubbard (Ed.), Marcel Dekker, New York, 2002, pp. 136–166.
[9] L.V.C Rees, D. Shen, in: H. van Bekkum, E.M. Flaningen, P.A. Jacobs, J.C. Jansen (Eds.), Introduction to zeolite science and practice, Elsevier, 2001.
[10] A. Rossner, S.A. Snyder, D.R.U. Knappe, Water Res. 43 (2009) 3787–3796.
[11] D.R.U. Knappe, A. Rossner, S.A. Snyder, C. Strickland, American Water Works Association Research Foundation, Denver, Colorado, 2007.
[12] I. Braschi, S. Blasioli, L. Gigli, C.E. Gessa, A. Alberti, A. Martucci, J. Hazard. Mater. 178 (2010) 218–225.
[13] M.A. Anderson, Environ. Sci. Technol. 34 (2000) 725–727.
[14] A. Martucci, L. Pasti, M. Nassi, A. Alberti, R. Arletti, R. Bagatin, R. Vignola, R. Sticca, Microporous Mesoporous Mater. 151 (2012) 358–367.
[15] L.I. Abu-Lail, Removal of chloroform and MTBE from water by adsorption onto granular zeolites: equilibrium, kinetic and mathematical modeling study, A Dissertation in Civil and Environmental Engineering, Worcester Polytechnic Institute, Department of Civil and Environmental Engineering, 2010.
[16] H.W. Hung, T.F. Lin, J. Hazard. Mater. B 135 (2006) 210–217.
[17] D. Zadaka-Amir, A. Nasser, S. Nir, Y.G. Mishael, Microporous Mesoporous Mater. (2011)http://dx.doi.org/10.1016/j.micromeso.2011.10.033.
[18] OEHHA, California, 1999, p. 136.
[19] W.M. Meier, Z. Kristallogr. 115 (1961) 439–450.
[20] S.M. Csicsery, Zeolites chemistry and Catalysis, ACS Monographs 171, American Chemical Society, Washinton DC, 1976.
[21] A. Alberti, P. Davoli, G. Vezzalini, Z. Kristallogr. 175 (1986) 249–256.
[22] A.C. Larson, R.B. Von Dreele, GSAS-General Structure Analysis System, Report LAUR 86–748, Los Alamos National Laboratory, Los Alamos, New Mexico, 1996.
[23] B.H. Toby, J. Appl. Crystallogr. 34 (2001) 210–213.
[24] A. Martucci, L. Pasti, N. Marchetti, A. Cavazzini, F. Dondi, A. Alberti, Microporous Mesoporous Mater. 148 (2012) 174–183.
[25] P. Thomson, D.E. Cox, J.B. Hastings, J. Appl. Crystallogr. 20 (1987) 79–83.
[26] A. Erdem-Senatalar, J.A. Bergendahl, A. Giaya, R.W. Thompson, Environ. Eng. Sci. 21 (2004) 722–729.
[27] J.P. Mota, S. Lyubchik, Recent Advances in Adsorption Processes for Environmental Protection and Security NATO Science for Peace and Security, Series C: Environmental Security, Springer, The Netherlands, 2008.
[28] A. Giaya, R.W. Thompson, R. Denkewicz Jr., Microporous Mesoporous Mater. 40 (2000) 205–218.
[29] B.A. De Moor, M.-F. Reyniers, O.C. Gobin, J.A. Lercher, G.B. Marin, J. Phys. Chem. C 115 (2011) 1204–1219.
[30] P. Simoncic, T. Armbruster, Am. Mineral. 89 (2004) 421–431.
[31] Yu.L. Slovokhotov, T.V. Timofeeva, M.Yu. Antipin, Yu.T. Struchkov, J. Mol. Struct. 112 (1984) 127–140.
[32] Ch. Baerlocher, L.B. McCusker, D.H. Olson, Atlas of Zeolite Framework Types, Sixth revised Ed., Elsevier, Amsterdam, 2007.